Radar Observations of the 3 May 1999 Oklahoma City Tornado

DONALD W. BURGESS

National Severe Storms Laboratory, Norman, Oklahoma

MICHAEL A. MAGSIG

Cooperative Institute for Mesoscale Meteorological Studies and NWS Warning Decision Training Branch, Norman, Oklahoma

JOSHUA WURMAN

School of Meteorology, The University of Oklahoma, Norman, Oklahoma

DAVID C. DOWELL*

National Severe Storms Laboratory and Cooperative Institute for Mesoscale Meteorological Studies, Norman, Oklahoma

YVETTE RICHARDSON

School of Meteorology, The University of Oklahoma, Norman, Oklahoma

(Manuscript received 23 March 2001, in final form 14 December 2001)

ABSTRACT

The 3 May 1999 Oklahoma City storm is unique from a weather radar perspective because a long-track violent tornado passed within close range of several Doppler radars, because a detailed damage survey was conducted immediately after the event, and because high-quality visual observations of the tornado were available. The tornado passed relatively close (15–60 km) to two fixed-location Doppler radars: the National Weather Service Weather Surveillance Radar-1988 Doppler (WSR-88D) at Twin Lakes (KTLX) and the Radar Operations Center WSR-88D test radar at Norman (KCRI). Two mobile Doppler on Wheels (DOW) radars also observed the tornado at very close range (3–8 km). The data from DOW2 are nearly continuous for a substantial portion of the tornado's life and provide detailed information on the high-resolution velocity field in and around the tornado. These data permit good estimates of tornado rotational velocity and diameter. The data also allow comparison with tornado damage survey estimates of damage/intensity and with visual observations of tornado size. Further, one can compare the high-resolution DOW data to the lower-resolution WSR-88D observations to determine how much tornado information is lost because of the broader beamwidth (longer range) and longer gate length of the WSR-88Ds. Results of the study will be useful in determining how better to interpret future WSR-88D observations of near-range tornadoes, including any possible real-time estimation of tornado intensity and evolution.

1. Introduction

The 3 May 1999 Oklahoma City, Oklahoma, storm is unique from a weather radar perspective because a long-track violent tornado passed within close range of several Doppler radars, because a detailed damage survey was conducted immediately after the event, and because high-quality visual observations of the tornado were available. Having multiple radars at close range to a large tornado affords an opportunity to investigate 1) the structure and evolution of the tornado and the rotational flows surrounding it, 2) the relationship of the radar signatures to tornado damage/intensity, and 3) radar sampling issues associated with tornadoes and the complex flow within which they are embedded.

With the availability of such a rich dataset and with many important scientific questions to pursue, we plan a series of articles on this case. This paper examines the evolution of reflectivity and velocity signatures of the tornado and discusses issues associated with radar sampling of the small scales. Other papers envisioned for the future will examine the larger scales of rotation and storm dynamics and the comparison between de-

* Current affiliation: National Center for Atmospheric Research, Boulder, Colorado.

Corresponding author address: Donald W. Burgess, National Severe Storms Laboratory, 1313 Halley Circle, Norman, OK 73069.
E-mail: donald.burgess@noaa.gov

tailed radar and photogrammetric analyses. Another topic that will be left to a later paper is the maximum wind speed produced by the Oklahoma City tornado. The maximum wind speed likely occurred during the early portion of the tornado's life. This paper will emphasize the middle portion of the tornado's life when radar observations are most complete and when the damage survey F-scale estimates are most reliable.

Section 2 of this paper is a short summary of the tornado track. Section 3 presents a discussion of the Doppler radar observations that were collected on 3 May 1999. Section 4 describes the Oklahoma City tornado reflectivity signatures seen by the radars. Section 5 describes the Oklahoma City tornado velocity signatures seen by the radars. Section 6 discusses issues associated with the velocity signatures and suggests possible ways to use the signatures in estimation of tornado strength and evolution and in tornado warnings. Section 7 summarizes our conclusions.

2. Tornado track

For several days, beginning on the morning of 4 May 1999, as many as seven damage survey teams from the Norman meteorological community and Texas Tech University completed a careful documentation of damage from the Oklahoma City tornado, including estimation of F-scale intensities (Fujita 1971). Three of the teams were from Texas Tech University, and a summary of their surveys is given by Gardner et al. (2000) and Marshall (2002). The other four survey teams were from the Norman meteorological community [the Norman National Weather Service (NWS) Forecast Office, the National Severe Storms Laboratory (NSSL), the Storm Prediction Center, and the NEXRAD Radar Operations Center (ROC)]. The Texas Tech surveys and the Norman community surveys were combined to produce a detailed contour map of F-scale ratings for the Oklahoma City tornado (Fig. 1). Times along the path were calculated from known damage times and radar positions of tornado signatures. The high quality of the damage survey allowed F-scale increments to be further subdivided. For example, in later figures, stronger F2, F3, and F4 damage will be given F2.5, F3.5, and F4.5 designations.

The Oklahoma City tornado was the ninth in a series of 14 tornadoes produced by supercell A of the outbreak [see Speheger et al. (2002) for a mapping of all tornadoes in the outbreak]. Tornado 9, the Oklahoma City tornado, began near Amber, Oklahoma, at 2326:30 (all times are UTC; a start time of 2327 has been arbitrarily chosen). It traveled northeast, growing wide and intense, and striking Bridge Creek, Oklahoma, about 2350 (Fig. 1). The tornado narrowed and weakened between 0005 and 0015 before again widening somewhat and regaining intensity as it struck southwest Oklahoma City and Moore, Oklahoma, between 0020 and 0030. The tornado remained intense (but not nearly as wide as it had been near Bridge Creek) as it turned more northerly, striking southeast Oklahoma City, Del City, and Midwest City, Oklahoma. The tornado dissipated at 0047 after traveling 61 km in 80 min. The latter one-third of the track (after 0017) was primarily through urbanized neighborhoods with many houses and other structures (public and commercial buildings). Damage to those structures, with known building codes, gave the most accuracy in estimating the F-scale rating.

3. Doppler radar observations

a. WSR-88D data

The use of fixed-location Doppler radars in detecting tornadoes and the circulations surrounding them dates back to the 1950s and early 1960s [see Donaldson (1990) for a summary]. Burgess et al. (1993) more recently summarized techniques and limitations of detecting tornadoes with Doppler radar. The Next-Generation Doppler Radar (NEXRAD) program and the Weather Surveillance Radar-1988 Doppler (WSR-88D) network, currently used by the NWS to issue warnings, are documented by Crum and Alberty (1993).

Important operating characteristics of the WSR-88Ds are given in Table 1. Scans of the Oklahoma City tornado were available from two radars: the central Oklahoma operational WSR-88D (KTLX) located about 8 mi northeast of Norman, and the ROC test WSR-88D (KCRI) located in north Norman. WSR-88D Level-II data were analyzed with the WSR-88D Algorithm Testing and Display System (WATADS; NSSL 2000), which featured an automatic dealiasing algorithm. In general, improperly dealiased data were not a problem during the analysis. Spectrum-width data were used as data quality indicators. Velocities from sample volumes with very large spectrum width (indicative of poor mean velocity estimation) were not used in the analysis.

During its lifetime, the tornado was 17–59 km (9–32 n mi) from KTLX and KCRI. Lowest elevation angle (0.5°) beam centerline heights were 300 m–1 km (1000–3300 ft) AGL. The KTLX radar, which was operated in volume coverage pattern (VCP) 11 (scans at elevation angles up to 19.5° with updates every 5 min), collected data continuously during the tornado. The KCRI radar, which was operating in a test mode with an azimuthal sampling interval of 0.5° (Brown and Wood 2000) did not collect data continuously. Complete time–height histories of the KTLX reflectivity and velocity signatures were obtained. These signatures were compared with those in the KCRI data. Because the radar depictions are similar, only limited KCRI data will be presented.

b. DOW data

The use of mobile Doppler radars to detect and to study tornadoes and surrounding circulations began during the late 1980s. The first mobile Doppler radar to be

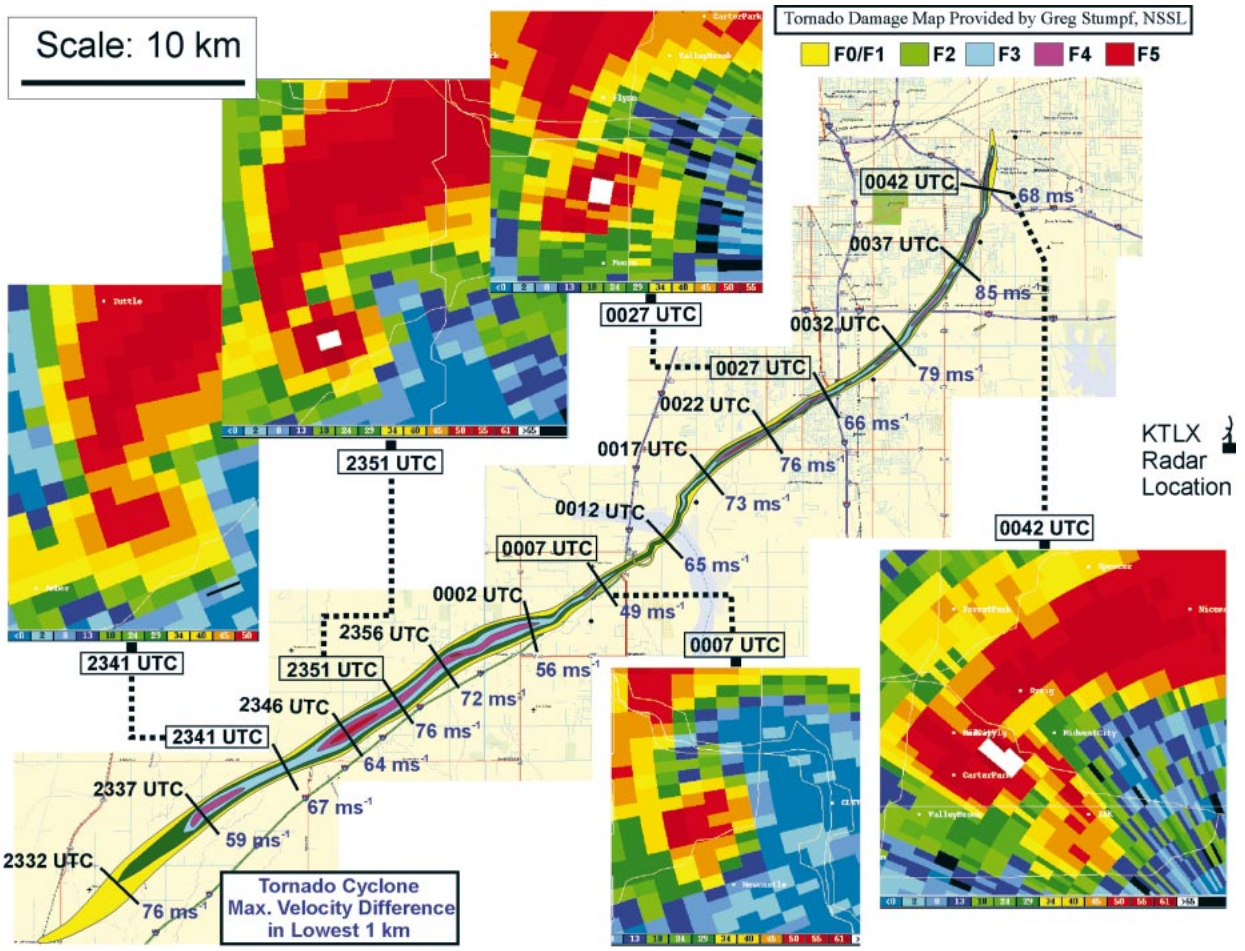

FIG. 1. Oklahoma City tornado damage track. Time and velocity difference (Delta-V; m s^{-1}) for KTLX WSR-88D tornado cyclone signature is marked. KTLX WSR-88D hook echo at selected times is inserted. Location of KTLX radar is marked.

used in tornado probing was a 3-cm continuous-wave Doppler radar (Bluestein et al. 1993). The first 3-mm, mobile, pulsed-Doppler radar to be used in tornado research was described by Bluestein et al. (1995). Recent 3-mm radar measurements for a tornado with supercell A that preceded the Oklahoma City tornado on 3 May were reported by Bluestein and Pazmany (2000). The first 3-cm, mobile, pulsed-Doppler radars to be used in tornadic storm and tornado research were the Doppler on Wheels (DOWs; Wurman et al. 1996, 1997). Wurman and Gill (2000, hereinafter WG) recently published the first finescale observational study of most of the life cycle of a tornado (near Dimmit, Texas, on 2 June 1995), using a DOW. The DOWs currently are being used to study another of the 3 May tornadoes—the Mulhall, Oklahoma, tornado (Wurman 2002).

TABLE 1. WSR-88D and DOW radar characteristics.

Parameter	WSR-88D	DOW
Wavelength	10 cm	3 cm
Transmitted peak power	750 kW	250 kW
Nyquist velocity	±34 m s^{-1}	±21 m s^{-1}
Stationary beamwidth	0.95°	0.93°
Rotating (effective) beamwidth	1.25°	1.07°
Azimuthal sample interval	1.0°	0.5°
Range gate spacing (velocity/reflectivity)	250 m/l km	50 m/50 m
Elevation angles	0.5°–19.5°	~0.5°–18°
Data interval	5 min	1 min
Range to tornado	17–59 km	3–8 km
Low beam height	300 m–1 km	50–150 m

Important operating characteristics of the DOWs on 3 May are given in Table 1. DOW data used in this paper were analyzed with Solo (Oye et al. 1995). Solo is software to edit and to display radar data in polar format. It was developed at the National Center for Atmospheric Research (NCAR). No automatic dealiasing algorithm was used. DOW pulse repetition frequencies (PRFs) gave a Nyquist velocity measurement interval of ± 21.3 m s^{-1}. Because wind speeds in and around the tornado greatly exceeded the measurement interval, many velocity measurements were aliased. Manual dealiasing was employed to calculate DOW-measured velocities in the tornado. DOW reflectivities were not completely calibrated and may have had errors because of receiver saturation when close to a high-reflectivity feature. In similar fashion to WSR-88D analysis, DOW spectrum-width data were used as data quality indicators. Velocity estimates with very large spectrum widths were not used in the DOW analysis.

Two DOWs (DOW2 and DOW3) observed the tornado during its lifetime at very close range (3–8 km). Data from DOW2 were nearly continuous and contained sector scans with elevation angles to 18° (1-min volume updates) for a substantial portion of the tornado's life. The time period of 0000–0033 UTC, a subset of the tornado's lifetime and shorter than the analysis period for the WSR-88D data, was selected for intensive study. Both DOWs were moving almost all of the time during the analysis period to keep up with the tornado. This movement added complexity to the analysis. Some, mostly lower, elevation angles were blocked by nearby buildings, trees, and terrain. Derived heights for indicated elevations were incorrect if the vehicles were moving uphill or downhill. Indicated beam heights were also incorrect for uneven/tilted road surfaces on which the pedestal was not level. Continuity of signatures was used to detect and to exclude data associated with incorrectly indicated elevation angles. Some subjectivity was necessary in both the velocity dealiasing and in the correction of elevation angles. Although a number of data points were removed, some residual error may still be contained within the dataset. Time–height histories of reflectivity and velocity signatures were made for DOW2 and checked against the intervals when DOW3 data were available. DOW3 data did include 1 min (0012–0013) of dual-PRF data collection (Nyquist measurement interval of ± 79 m s^{-1}). Because DOW3 data (including the dual-PRF segment) appear to be consistent with the DOW2 data, all DOW figures and results shown in this paper will be from DOW2.

Having a complete time–height history of the reflectivity and velocity signatures from KTLX and a substantial time period of time–height history from DOW2 affords an opportunity to investigate how the radar signatures relate to tornado existence, strength, and damage. It is also possible to compare the high-resolution DOW2 signatures to the lower-resolution KTLX signatures. Radar sampling issues associated with detection of tornadoes by WSR-88Ds can be studied in this context.

c. Radar sampling of tornadoes

Three radar sampling issues are especially relevant to our study of the Oklahoma City tornado: 1) the size and location of the tornado relative to the size and spatial distribution of the radar pulse volumes (Brown et al. 1978; Burgess et al. 1993; Wood and Brown 1997), 2) centrifuging of radar scatterers by the tornado (WG; Dowell et al. 2001), and 3) differential power weighting of the velocity spectrum in regions with strong reflectivity gradients (Bluestein et al. 1993). In most observations of tornadoes, such as those collected by the KTLX radar in the Oklahoma City storm, the vortex core is narrower than the effective radar beamwidth. The signature of the tornado in the radar data thus depends greatly on the characteristics of the flow surrounding the core and on the positions of the radar beams relative to the vortex center (Brown et al. 1978; Wood and Brown 1997). In contrast, in the scans at very close range to the Oklahoma City tornado by the DOW, the tornado core spans several adjacent radar beams. From a few 100 m AGL upward, tornadoes are typically associated with a minimum in reflectivity (often called an eye) in high-resolution radar scans (e.g., Fig. 2). Centrifuging of radar scatterers probably explains the minimum in reflectivity within the tornado core (WG; Dowell et al. 2001). When centripetal accelerations are large, the motion of radar targets such as precipitation and debris may differ significantly from the air motion.

Dowell et al. (2001) estimated the magnitude of the difference between the scatterer motion and the air motion (i.e., the measurement error) in a simple one-dimensional model; the prescribed air motion in the simulation is that of a Rankine combined vortex. Radar scatterers within the vortex move outward relative to the air. Furthermore, because the radar targets pass quickly through the region of strongest tangential winds at the edge of the core, the drag force exerted on the targets by the air does not have time to accelerate the targets to the peak air speed. Radar measurements of scatterer motion at the edge of the vortex core are thus overestimates of radial air velocity and underestimates of tangential air speed. The magnitude of the measurement error as a result of centrifuging in the one-dimensional model depends on the characteristics of the scatterer, the diameter of the vortex core, and the magnitude of the maximum tangential wind. Because weak-echo ''eyes'' in DOW observations of tornadoes typically form within preexisting regions of relatively high reflectivity that are connected to the main storm echo, we believe that the dominant scatterers in most DOW scans of tornadoes are precipitation (rain and/or hail). However, some tornadoes, such as the Oklahoma City tornado, generate such a large quantity of debris that this kind of scatterer may dominate at low levels. Using the

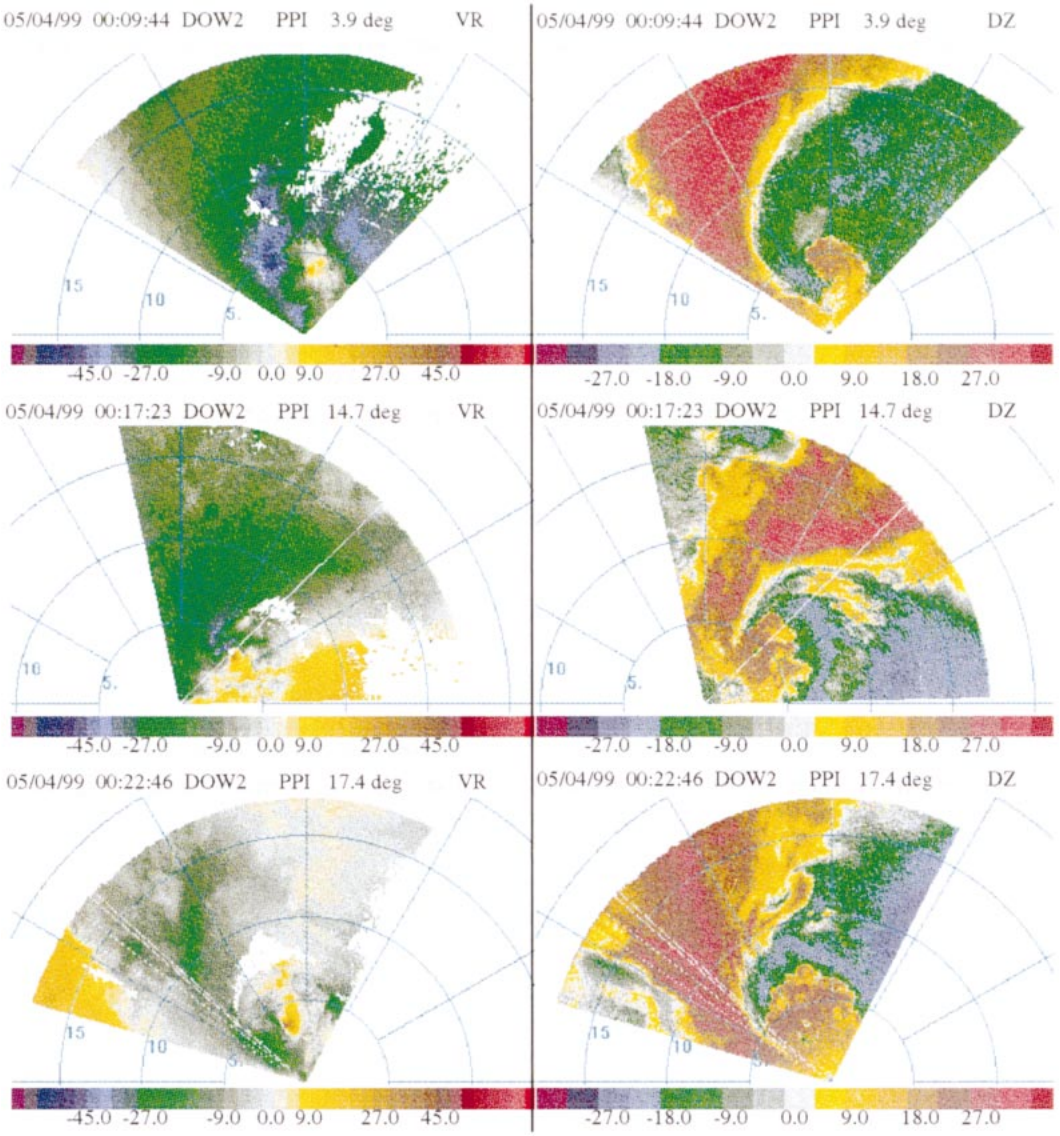

FIG. 2. DOW radar overview. (left) Velocity and (right) reflectivity for three times and elevations. Time (UTC) and elevation angle are marked in each panel.

referenced method, we estimated the measurement error of the maximum tangential wind speed for this case. The error may be as little as 4%, if the dominant scatterers were small raindrops, or as large as 40%, if the dominant scatterers were hail and/or large pieces of dense debris. However, because the cusp in the tangential velocity profile at the edge of the Rankine vortex in the simulation may be unrealistically sharp, the results should be considered as an upper bound on the magnitude of the measurement error.

Nonuniformity of the reflectivity distribution within the tornado (Bluestein et al. 1993) may further hinder the ability of the radar to resolve the velocity structure of the tornado. When radial air motions are weak [e.g., in that portion of the tornado above the surface layer (Lewellen 1993)], centrifuging removes scatterers from the vortex core and produces a high-reflectivity ring well outside the radius of maximum tangential wind (Dowell et al. 2001). For a broad radar beam straddling the edge of the core, the power-weighted mean velocity would be biased by the slower scatterer speeds in the high-reflectivity ring outside the radius of maximum winds. Thus, centrifuging indirectly contributes to further underestimation of the peak wind speeds in the tornado.

4. Reflectivity signatures

a. WSR-88D sampling

A well-defined hook was present with the supercell and had been in existence for 1.5 h at the time of the

beginning of the Oklahoma City tornado (see Fig. 1 insets for close-ups of the hook area and Fig. 3 for a wider view of the echo at selected times). Throughout the tornado's life, the hook featured a prominent ''knob'' that defined the location of the tornado and surrounding flow. Figure 4 is a time–height depiction of the maximum reflectivity in the knob and in the echo area above the top of the knob. Higher reflectivities in the knob (>55 dB*Z*) began near 2350 (near the time Bridge Creek was struck), extended up to heights above 2 km above radar level (ARL), and continued until the beginning of the weakening period about 0005. The higher reflectivities in the knob began again just after 0015, grew upward, and continued through the rest of the tornado's life. During the period of the latter reflectivity maximum, the tornado traveled almost exclusively through populated areas (the Oklahoma City metropolitan area), with large amounts of debris being generated. The second knob maximum was more reflective (70 dB*Z*) and extended to higher heights (at least 4 km) in comparison with the first maximum. In fact, the 70-dB*Z* values were 10 dB*Z* higher than the reflectivities present anywhere else in the storm during the same period (see Fig. 3 for a broader view of storm reflectivity).

The knob feature has long been seen in association with tornado-bearing hook echoes (Garrett and Rockney 1962) and has been related to tornadic velocity signatures (Lemon et al. 1982). We postulate that the localized reflectivity maximum in the knob of the hook emanates from large amounts of debris being lofted by the tornado. Tornado debris lofting to high heights and its subsequent long-distance transport have been discussed previously (Magsig and Snow 1998). The current observations extend the analysis to the interior of the storm. All this suggests that the existence of very large reflectivity in the knob of the hook can be used to infer that a tornado is present and is inflicting significant amounts of damage to structures.

b. DOW sampling

Because the DOWs were very close to the tornado, the radar data depict the hook echo in great detail (Fig. 2). At some intermediate elevation angles in the WSR-88D data (not shown), there was evidence of a minimum or eye of weaker reflectivity, which was surrounded by an annulus of much stronger reflectivity. This signature was easily seen in the DOW data as the center of the tornado (see Fig. 2) and has been reported previously (WG). It appears the eye may also be indicative of the absence of significant multiple vortices (Wurman 2002). Figure 5 is a time–height history of the reflectivity deficit within the eye feature as detected by DOW2. Observations below 300 m AGL typically did not indicate an eye. Concentration of scatterers by horizontal convergence in the vortex surface layer and generation of new scatterers at the surface (i.e., debris) may be responsible for the high radar reflectivity within the vortex core near the surface.

At heights near 300 m, the diameter of the minimum in reflectivity associated with the tornado was less than 100 m; at higher heights, its diameter was larger. Near the top of some DOW VCPs (>1.5 km ARL), the diameter of the minimum increased to over 500 m. The velocity data (next section) indicate that the tornado diameter increased with height. The diameter of the reflectivity minimum corresponds well with the diameter of the maximum tornado velocity. The eye feature aloft, at times, had minimum values that were more than 40 dB lower than the surrounding high-reflectivity annulus (Fig. 5). The eye's sharp reflectivity gradients (20–40 dB over a few hundred meters of horizontal distance) imply potential sampling problems associated with differential power weighting within the beam (section 3c).

5. Velocity signatures

a. WSR-88D sampling

The traditional tornado proxy of strong and localized velocity difference in radar sample volumes at the same range and adjacent azimuths (tornadic vortex signature: TVS; Burgess et al. 1993) does not apply in the Oklahoma City tornado case. This was because the maximum velocity difference in the tornado vicinity was separated across several azimuths (see Fig. 3 velocity insets). By taking the maximum velocity difference across a horizontal distance of less than 1.85 km, a small-scale couplet was identified and will be referred to as a tornado cyclone signature (TCS). The term tornado cyclone has been applied previously to circulations larger than the tornado as inferred from tornado damage patterns (Agee et al. 1976) or resulting from numerical model studies (Wicker and Wilhelmson 1993). The TCS at low elevation angles, for which the radar beam height was less than 1 km ARL, corresponded relatively well to tornado location, and the trend in its magnitude was similar to that of the tornado F scale (Fig. 1 plotted values, and Fig. 6). The TCS velocity difference (called Delta-V) rapidly exceeded 45 m s^{-1} as the tornado formed and stayed large (near 70 m s^{-1}) during the time period when the tornado was at F5 intensity (2345–2350 and near 2355; Fig. 6). Delta-V lessened to below 50 m s^{-1} as the intensity dropped to F2. Delta-V quickly increased again and stayed strong (70–85 m s^{-1}) during the rest of the life of the tornado as the intensity returned to F5 (0020–0023 and near 0026) and strong F4. The latter peak was during the tornado's passage through the southern and southeast portions of the metropolitan area. Delta-V values remained large and tornado intensity remained high until the last 2 or 3 min of the tornado's life, when the tornado weakened rapidly.

A time–height section of TCS Delta-V (Fig. 7) reveals that values were already somewhat large before tornado formation (greater than 40 m s^{-1}) but were stronger aloft

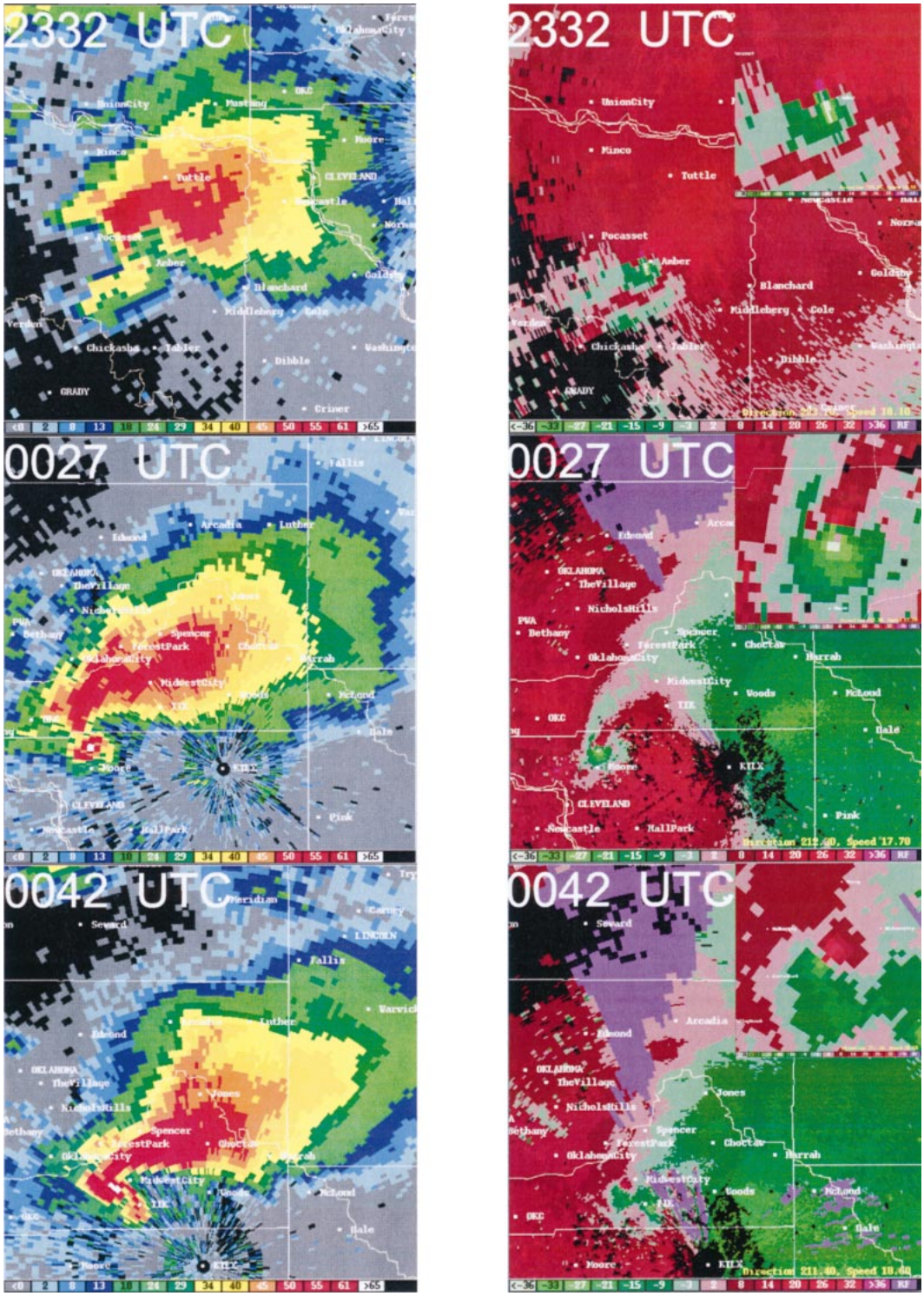

FIG. 3. (left) The 0.5° KTLX WSR-88D reflectivity and (right) storm-relative velocity for three times during the Oklahoma City tornado. Inset in upper-right portion of velocity images is magnified view of rotation signature region.

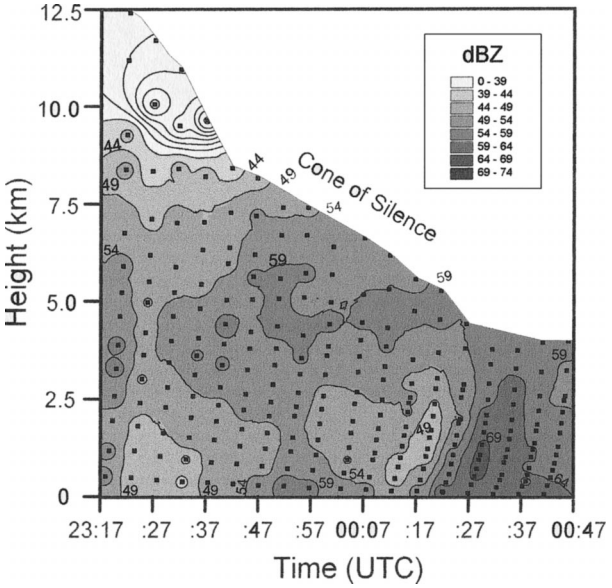

FIG. 4. Time–height diagram of KTLX WSR-88D maximum reflectivity in and above the hook echo. The ''cone of silence'' that vertically limits data collection is marked.

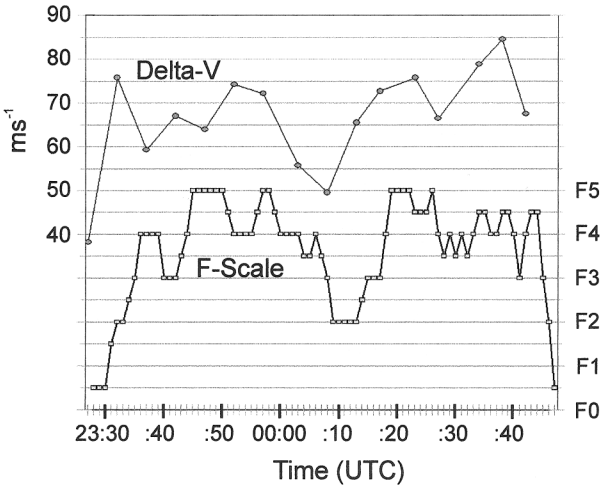

FIG. 6. Graph of KTLX WSR-88D tornado cyclone Delta-V (m s^{-1}) in lowest kilometer and F-scale rating.

and weaker near the ground. Very large values (greater than 45 m s^{-1}) formed through a deep column as the tornado formed (2327). The large Delta-V values continued until about 0000; maximum values remained at heights below 2.5 km ARL. Strengthening occurred again about 0015, and a deeper column of very large Delta-Vs continued until rapid weakening at tornado end. Measurement of the vertical extent of the second maximum of high Delta-V values is limited by the radar ''cone of silence'' produced when the storm approached the radar and the highest elevation angle (19.5°) intersected the circulation at heights lower than 5 km ARL. Although the column of very large Delta-Vs was deep, the highest Delta-V values (greater than 75 m s^{-1}) were found at the lowest elevation angles.

Tornado cyclone diameter (Fig. 8) as estimated by KTLX is greatly affected by range to the tornado: largest near the beginning when the tornado was farthest from the radar, and smallest near the end when the tornado was closest to the radar. Low-level TCS diameters were larger than diameters aloft. The decreasing diameter with height is inconsistent with numerical vortex models

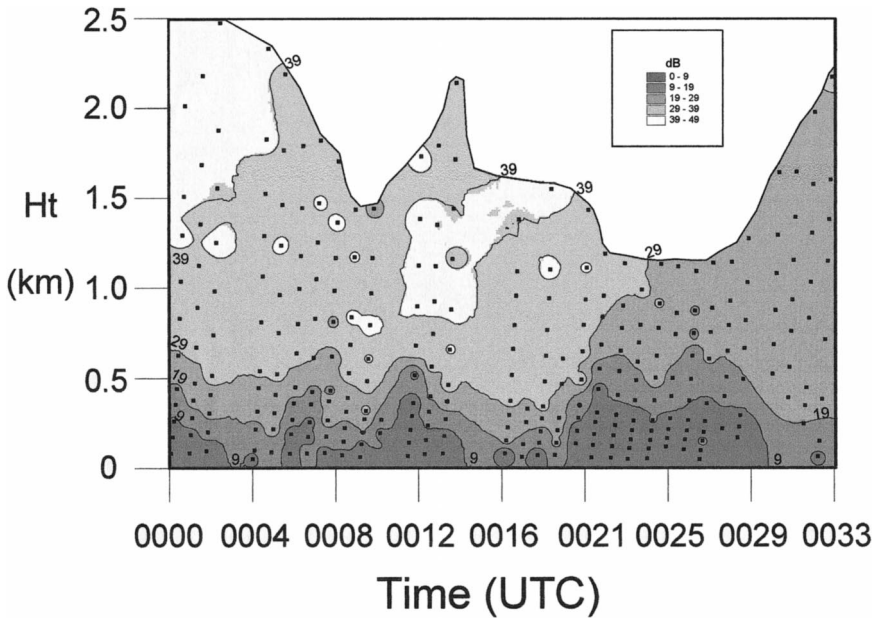

FIG. 5. Time–height plot of DOW magnitude of tornado eye. Plotted value is reflectivity in the annulus minus reflectivity in the center of the eye.

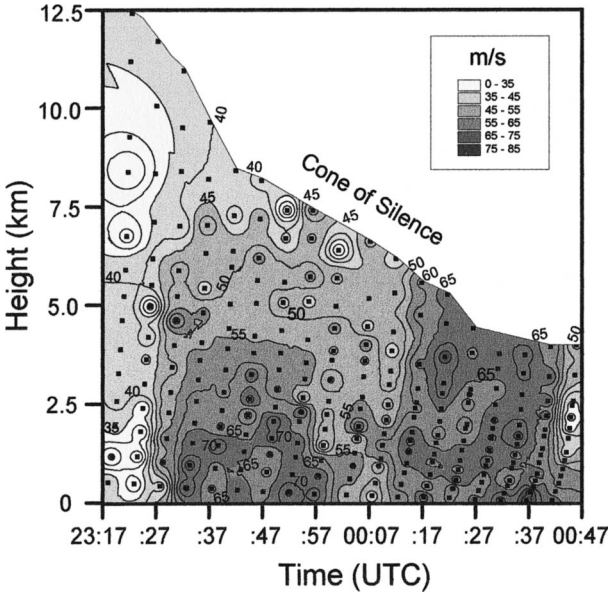

FIG. 7. Time–height plot of KTLX WSR-88D tornado cyclone Delta-V.

(Lewellen 1993), which would suggest that tornado and TCS diameters would increase with height. DOW observations (section 5b) indicate increasing tornado diameter with height.

b. DOW sampling

The DOW data from 0000 to 0033 have been analyzed in several ways. The first analysis is of the highest ground-relative velocity close to the ground (height <150 m ARL). The velocity is derived by using Delta-V to estimate rotational velocity and adding vortex motion (see Table 2). Vortex motion was determined from WSR-88D data. Good low-level tornado wind speed estimates were not obtained for all low-level scans because of DOW movement and blockage by objects along the road. The trend in the tornado speed estimates is similar to that in the F-scale estimates (Fig. 9), and the results do not seem to be biased by height within the 50–150-m interval. At the beginning of the analysis period (near 0000), the wind speed is relatively strong (near 80 m s^{-1}) when F4 damage was occurring. As the

TABLE 2. Calculation of DOW low-level (LL) tornado wind speed.

Time (UTC)	Height (m)	LL Delta-V (m s^{-1})	LL rotational velocity (m s^{-1})	Tornado motion (m s^{-1})	LL tornado wind speed (m s^{-1})
0000	85	135	67.5	13.7	81
0001	87	135	67.5	13.7	81
0002	98	127	63.5	13.7	77
0004	101	126	63	13.7	77
0005	93	126	63	13.1	76
0006	83	136	68	13.1	81
0007	84	116	58	13.1	71
0008	88	96	48	13.1	61
0009	73	98	49	13.1	62
0010	64	100	50	13.1	63
0012	71	92	46	11.3	57
0013	81	89	44.5	11.3	56
0014	84	89	44.5	11.3	56
0017	84	117	58.5	11.8	70
0018	65	121	60.5	11.8	72
0019	75	125	62.5	11.8	74
0020	143	124	62	11.3	73
0021	133	157	78.5	11.3	90
0022	59	159	79.5	11.3	91
0023	52	168	84	11.3	95
0024	112	157	78.5	11.3	90
0026	107	136	68	12.1	80
0027	50	116	58	12.1	70
0032	67	143	71.5	14.7	86

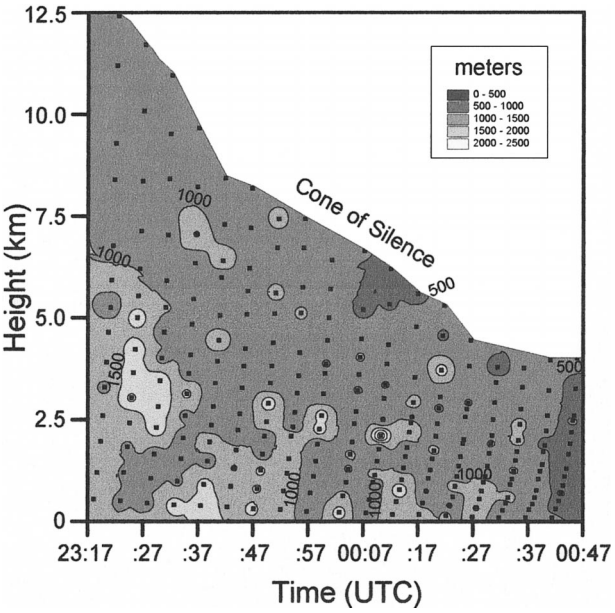

FIG. 8. Time–height plot of KTLX WSR-88D tornado cyclone diameter.

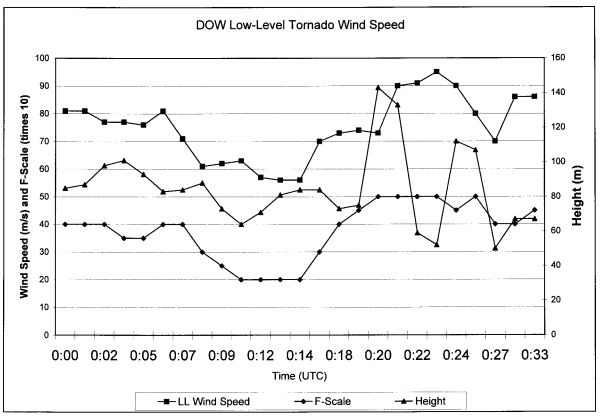

FIG. 9. Graph of DOW low-level tornado ground-relative wind speed, height of estimate, and F-scale rating.

TABLE 3. Wind speed estimates and damage descriptions of Fujita-scale categories (Fujita 1971).

Rating	Wind speed (m s^{-1})	Description
F0	18–32	Light damage: some damage to chimneys and TV antennas; twigs broken off trees; some shallow rooted trees pushed over
F1	33–50	Moderate damage: surface peeled off roofs, windows broken; light/unanchored mobile homes pushed or overturned; some trees uprooted or snapped; moving automobiles pushed off road
F2	51–70	Considerable damage: roofs torn off frame houses, leaving strong upright walls; weak buildings demolished; mobile homes destroyed; large trees snapped or uprooted; railroad boxcars pushed over; light-object missiles generated; automobiles blown off road
F3	71–92	Severe damage: roofs and some walls torn off frame homes; rural buildings completely demolished; trains overturned; steel frame warehouse/hanger structures destroyed; cars lifted off the ground; most trees in a forest uprooted, snapped, or leveled
F4	93–116	Devastating damage: whole frame homes leveled, leaving piles of debris; steel structures badly damaged; trees debarked by small flying debris; cars and trains thrown some distance or rolled considerable distance; large missiles generated
F5	117–142	Incredible damage: whole frame homes leveled, no debris left on foundation; steel-reinforced concrete structures badly damaged; automobile-sized missiles generated; incredible phenomena can occur

F-scale estimate weakens to F2 (just after 0010), wind speeds decrease to below 60 m s^{-1}. As strengthening to F5 occurs (near 0020), the wind speeds increase to over 90 m s^{-1}. As weakening to F3.5 occurs (near 0028), the wind speed estimates drop to about 70 m s^{-1}. As the F-scale rating strengthens again to F4.5, the wind speed estimates increase to over 85 m s^{-1}.

All of the wind speed estimates are lower than those associated with the Fujita scale (Table 3). It is tempting to suggest that these observations support recent conclusions by McDonald (2001) and Marshall (2002) that the wind speeds associated with the higher F numbers are too high. However, a number of factors make the comparison difficult. The Fujita scale associates damage with the fastest 0.25 mi of wind at 10-m height. Therefore, winds discussed by McDonald and Marshall apply to different heights and different wind averaging times/distances than do the radar observations. DOW winds are collected in a small fraction of a second and do not equate to averaging over 0.25 mi or several seconds. Second, it is possible that the highest wind speeds were below the beam heights of the DOW. Evidence in numerical simulations indicates that the strongest tangential winds in tornadoes tend to occur within a surface layer; this layer, in which interaction of the vortex with the ground results in strong radial inflow, may be shallower than 100 m for strong tornadoes (Lewellen 1993). Photogrammetric analyses of tornadoes (Hoecker 1960; Golden and Purcell 1977) have also indicated maximum wind speeds below 70 m AGL. The DOW sampled the winds at 50 m ARL and higher. Because the lowest scans by the DOW did not indicate significantly more radial inflow than in the scans aloft, we speculate that the boundary layer in the Oklahoma City tornado was too shallow to be sampled by the DOW. A third consideration in the evaluation of the maximum wind speeds in the Oklahoma City tornado is that radar scatterers tend to attain maximum tangential speeds that are less than the maximum air tangential speeds (section 3b). Last, radar estimates of wind speeds are power-weighted means within a volume; regions of strong wind speeds that are small and/or are within low reflectivity may not be resolved.

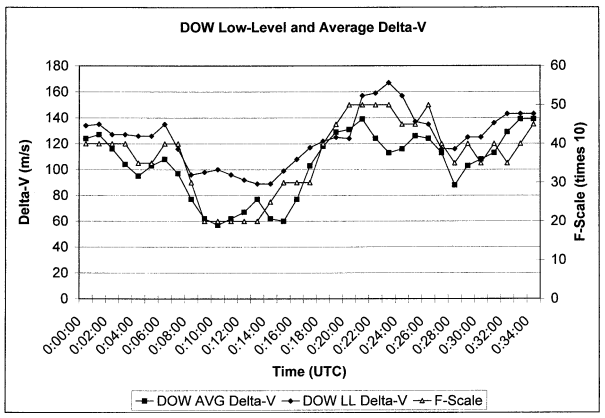

FIG. 10. DOW low-level and average Delta-V (m s^{-1}) and F-scale rating.

To aid in the comparison of the DOW data with the WSR-88D data, average low-level Delta-V values in the DOW data have been calculated (Fig. 10). The averaging is over a vertical layer centered on the height of the low-level WSR-88D beam and having a layer width comparable to the 1° WSR-88D vertical beamwidth; this is called the average Delta-V. The estimates of Delta-V at the lowest DOW level (Table 2) have also been included in Fig. 10. The trends in Delta-V are similar to those in the F-scale ratings. The two Delta-V curves are similar because of the vertical continuity of Delta-V values. Because the maximum Delta-V is almost always at the lowest level, the average Delta-V is almost always smaller than the low-level Delta-V. One exception is at 0020 when the average Delta-V is larger than the low-level Delta-V at a time when the F scale is increasing. This could result from a low-level estimate that is too small because of undetected beam misalign-

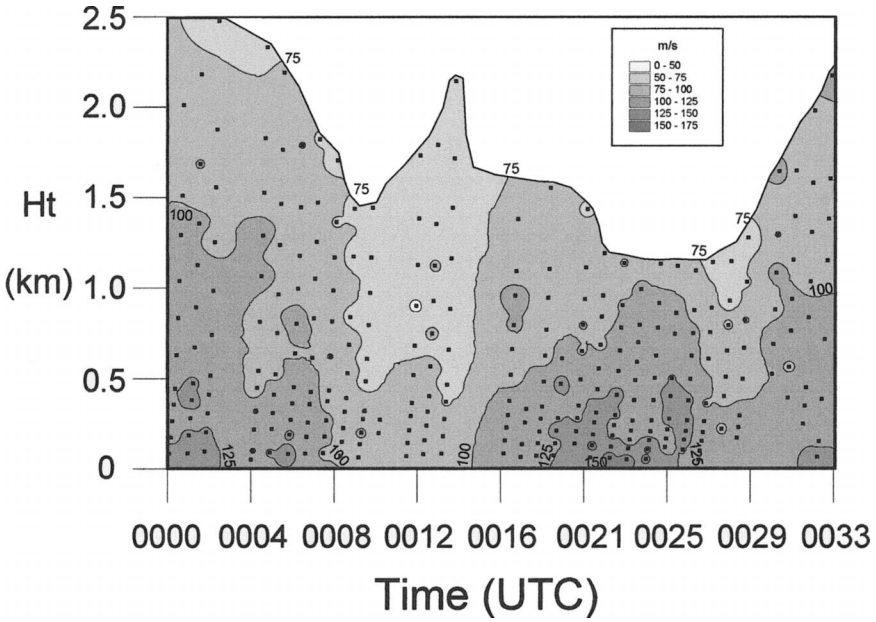

FIG. 11. Time–height plot of DOW Delta-V.

ment or incorrect dealiasing, or it could result from some natural phenomenon that caused the maximum to be elevated for a brief interval.

Height–time plots of DOW Delta-V (Fig. 11) and Delta-V diameter (Fig. 12) have also been analyzed. Delta-V is largest in the lowest 300 m ARL, and values drop by as much as 50% at heights of 1500 m and higher. The DOW tornado signature is still clearly defined aloft, but it has a lower wind speed. Early in the analysis period (0000–0005), there is a relatively tall column of stronger Delta-V. The 0008–0015 weakening of Delta-V is seen to occur at all levels. Strengthening of Delta-V after 0015 is again throughout the column, but the vertical extent of large values is not quite as high as for the earlier peak. The low-level maximum in Delta-V (0021–0024) is easily seen in the plot. The shorter-period weakening (0027–0030) is also seen, as well as the increasing trend at the end of the analysis (0033).

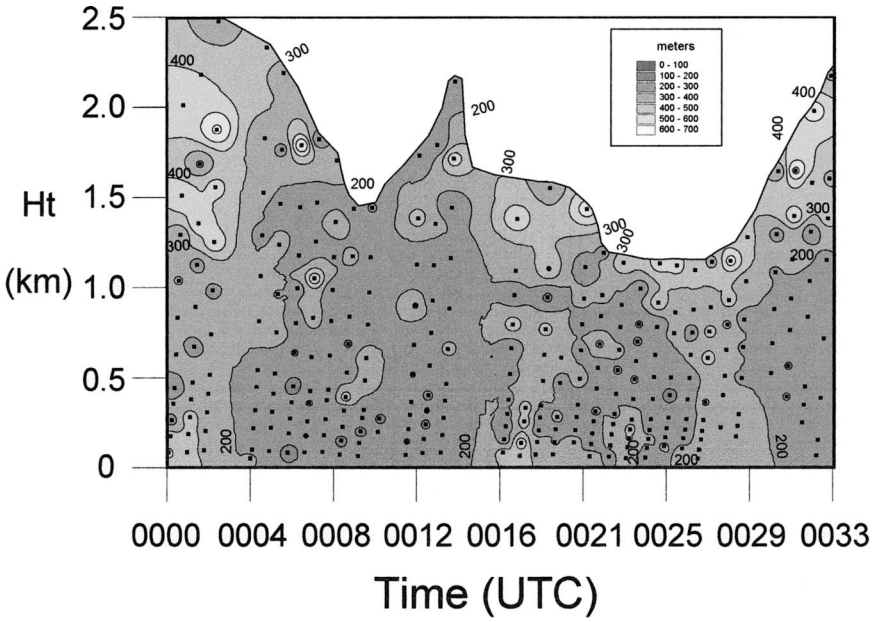

FIG. 12. Time–height plot of DOW tornado signature diameter (distance between locations of maximum inbound and outbound velocity).

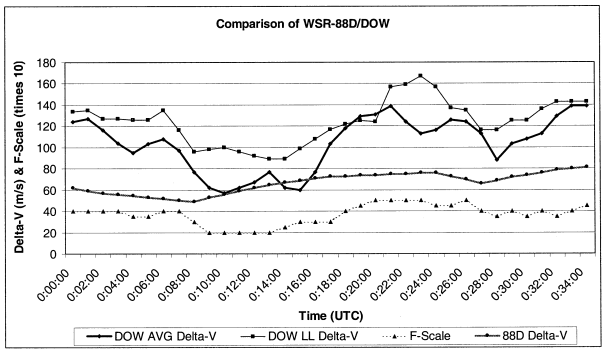

FIG. 13. Comparison of WSR-88D Delta-V, DOW low-level Delta-V, DOW average Delta-V, and F-scale rating. WSR-88D Delta-V values (5-min intervals) have been linearly interpolated to 1-min increments for plotting purposes.

In agreement with expansion of the eye feature with height (discussed previously), Delta-V diameter of the tornado is generally narrower near the ground and wider aloft (Fig. 12). Tornado diameter was wider at the beginning of the analysis (0000), with values of about 300 m near the ground and greater than 500 m aloft. The low-level diameter decreased to less than 200 m by about 0005 and stayed that narrow until just after 0015 when diameter widening and strengthening wind speeds occurred. The upper-level diameter also decreased to less than 200 m for a short interval (0011–0014). At the time of the peak low-level wind speeds (0020–0024), the low-level diameter was 200–300 m and the diameter aloft was again wider than 400 m. At the time of the last strengthening of wind speeds (0032–0033), the low-level diameter had narrowed to about 200 m, but the diameter aloft was still wider than 400 m.

6. Discussion of velocity signatures

a. Comparison of WSR-88D and DOW data

This dataset provides a unique opportunity to compare tornado wind estimates from two radars (Fig. 13): a fixed-location operational radar, at what would be considered close range to the tornado, and a mobile radar, driving at very close range to the tornado. As was shown in the last section, the DOW low-level and average Delta-Vs are comparable to each other (the low-level Delta-V generally being larger) and are consistent with changes in the F-scale rating. The WSR-88D Delta-V curve is 25–50 m s^{-1} less in magnitude and much smoother than the DOW curves, not depicting well the DOW maxima and minima, or changes in F-scale estimates (Fig. 13). Although there is general agreement between the WSR-88D Delta-V and F scale, the detailed changes are not detected well. The sharp decrease in DOW Delta-Vs observed between 0006 and 0008 is seen only as a gradual weakening. The WSR-88D Delta-V minimum at 0008 is improperly placed in time when compared with the DOW minima and the minimum in F scale (0010–0015). The sharp increases in DOW Delta-Vs between 0014 and 0021 are seen only as gradual increases that began earlier. The peak in DOW average Delta-V at 0021 and the peak in low-level Delta-V at 0023 compare well with the WSR-88D Delta-V peak at 0022. The WSR-88D minimum at 0028 compares well with the DOW minima at about the same time, but the sharp DOW decreases are not seen. The DOW Delta-V increases that occur from 0029 until the end of the data have trends that are comparable to the WSR-88D Delta-V increases that occur during the same period. It is interesting to note that the maximum WSR-88D Delta-V within the DOW analysis period is the last point (0033 and 0034). The WSR-88D curve is trending toward the overall peak value (85 m s^{-1}) that occurred at 0038. The observation that stronger velocities were recorded after 0033 as compared with the likely real peak at 0022–0024 is perhaps related to the tornado's distance from KTLX. That distance was 22 km at 0022, but had dropped to 16 km by 0038.

There are some general agreements between WSR-88D TCS diameter (Fig. 8) and DOW tornado signature diameter (Fig. 12). During the period of the DOW analysis, low-level diameters are qualitatively similar: TCS and tornado diameters were wider near the beginning of the analysis (0000); both diameters narrowed after 0005, before widening again about 0010 (KTLX) and 0015 (DOW). Some narrowing in both occurred during the period of maximum intensity (0020–0025), and widening of both occurred (0025–0029) before the decrease in diameter at the end of the analysis. The qualitative agreement between TCS and DOW diameter is less at the highest heights of the DOW data (1.5–2.5 km). In a quantitative sense, the TCS diameters do not compare well with DOW estimates of tornado diameter. DOW tornado diameters were more narrow near the ground and broader aloft; TCS diameters show the opposite trend with height. In general, TCS diameters are 3–5 times as wide as DOW tornado diameters near the ground, but only about 2 times as wide aloft. Reasons for the diameter ratio differences with height between the two radars are not understood but are likely related to sampling issues.

The comparison of observations suggests that the 3 May WSR-88D signatures are useful in a qualitative sense; the data may be used to suggest that the tornado might be weaker or stronger at certain times during its life, or that the overall circulation diameter might be widening or narrowing. It does not appear that the 3 May WSR-88D signatures are useful in a quantitative sense; the data may not be used to suggest that the wind speeds are in a certain range. The utility of the WSR-88D for evaluating changes in tornado intensity is also limited by the 5-min time between updates. The DOW observations indicate significant fluctuations in tornado intensity over shorter timescales.

b. WSR-88D sampling issues

The difficulty in relating close-range gate-to-gate WSR-88D velocity differences to the tornado merits further discussion. The traditional TVS gate-to-gate signature was absent for most KTLX and KCRI scans. One of the possible reasons for the lack of a typical gate-to-gate signature is that, at close range, the large diameter of the tornado might produce a signature spread across several azimuths. To check this possibility and to define better the velocity field in and around the tornado, the DOW data were examined. Comparison of DOW data with KTLX and KCRI data for two times (Fig. 14) indicates that the tornado diameter is significantly smaller than the WSR-88D Delta-V signature. This result holds even when taking into account the possibility that sampling of the tornado vortex along its centerline could produce a signature spread across three azimuths instead of two.

Some of the DOW data, particularly at 0013, indicate that there is a second well-defined signature (pair of velocity peaks) that is larger than the tornado (Fig. 14). The WSR-88D signature is really a sum of the tornado and the larger circulation. It may be that the WSR-88D returns are more related to the flow surrounding the tornado than the tornado itselt. If this is correct, the strength of the surrounding flow must be somewhat well correlated to the tornado strength to produce the generally good comparisons between the WSR-88D TCS and the tornado.

The velocity signatures shown in Fig. 14 can be compared with images of the tornado taken at approximately the same times as the Doppler scans. Figure 15 shows the visual appearance of the tornado at the two comparison times, 0012 and 0028. Surveys were conducted after the event using damage survey maps, a digital compass, and a global positioning system to determine the azimuth of selected objects in the image, the height of these objects, and the distances to the objects and the tornado from the photo site. The heights of the objects were projected to the range of the tornado, and the width of the condensation funnel was computed from the resulting image distance–to–actual distance scale. Figure 15 (left) displays an image of the tornado at approximately 0012. In agreement with DOW estimates of a smaller vortex at 0013 (peak wind diameter of just over 100 m), the condensation funnel/debris cloud appears to be relatively narrow (180 m). Also in agreement with DOW estimates of a bigger vortex at 0027 (peak wind diameter of 250–300 m), the condensation funnel/debris cloud (Fig. 15, right) appears to be much wider at 0028 (340 m) than at 0012.

Figure 15 includes depictions of the DOW and WSR-88D beamwidths. These comparisons would suggest that, even for a close-range tornado (e.g., the 20-km distance between KTLX and the tornado at 0027), the 1° WSR-88D beamwidth (and the 1.25° effective beamwidth) is larger than the diameter of peak winds. In fact, a comparison of the full F0–F1 damage width at 0027 with the Doppler velocity signature (Fig. 16) shows that the width of all damage (larger than the peak wind diameter) is about 1.5 beamwidths wide. The factors mentioned here strongly suggest that the peak winds will be poorly sampled and underestimated, just as was observed.

7. Summary

Operational WSR-88D signatures in reflectivity and velocity have been shown to be useful in detecting and tracking the 3 May Oklahoma City tornado. The data revealed a reflectivity signature with large dB*Z* values associated with debris. Such reflectivity signatures, when present in the knob of the hook, and when the signature is over a region in which much debris may be produced, can be used to infer the presence of a damaging tornado. The 3 May WSR-88D velocity signatures appeared to be on a scale slightly larger than the tornado and were related to the strength of the flow surrounding the tornado. Called a tornado cyclone, the observed signature depicted tornado location well and gave some qualitative idea of tornado strength.

Mobile radar observations, such as those taken at very close range to the 3 May Oklahoma City tornado by the DOWs, are very useful in measuring tornado characteristics such as peak wind speed and diameter. Despite potential problems associated with a moving vehicle (beam blockage and antenna not level) and data reduction (subjective dealiasing of massively folded velocities), DOW tornado diameter and wind speed estimates compare very well with diameter estimates and trends in damage/intensity ratings obtained separately from a detailed damage survey. During the DOW analysis interval (0000–0033 UTC), the tornado weakened from peaks that occurred before the analysis interval, strengthened to a peak at which F5 intensity/damage was reported, again weakened slightly, and then strengthened again toward another intensity peak that was beyond the analysis interval. Estimates of peak tornado wind speed (50–150 m above radar level) were about 95 m s^{-1}. Although very strong, the wind speed was less than has been proposed for F5 intensity. This suggests that the Fujita scale F4 and F5 wind speed estimates may be too high for typical examples of home construction. However, the DOWs may not have sampled the peak winds because larger debris, not traveling as fast as the wind, may dominate the returns and because the peak winds may be below the 50–150-m heights. More data collection, perhaps with narrow-beam millimeter-wavelength radars, will be necessary to resolve the wind field within the lower 100 m of tornadoes. Solutions to sampling problems like the dominance of radar returns from large debris traveling at less than the actual air motion will need to be found. Comparison of current wind speed estimates (including time–height sections) with numerically simulated tor-

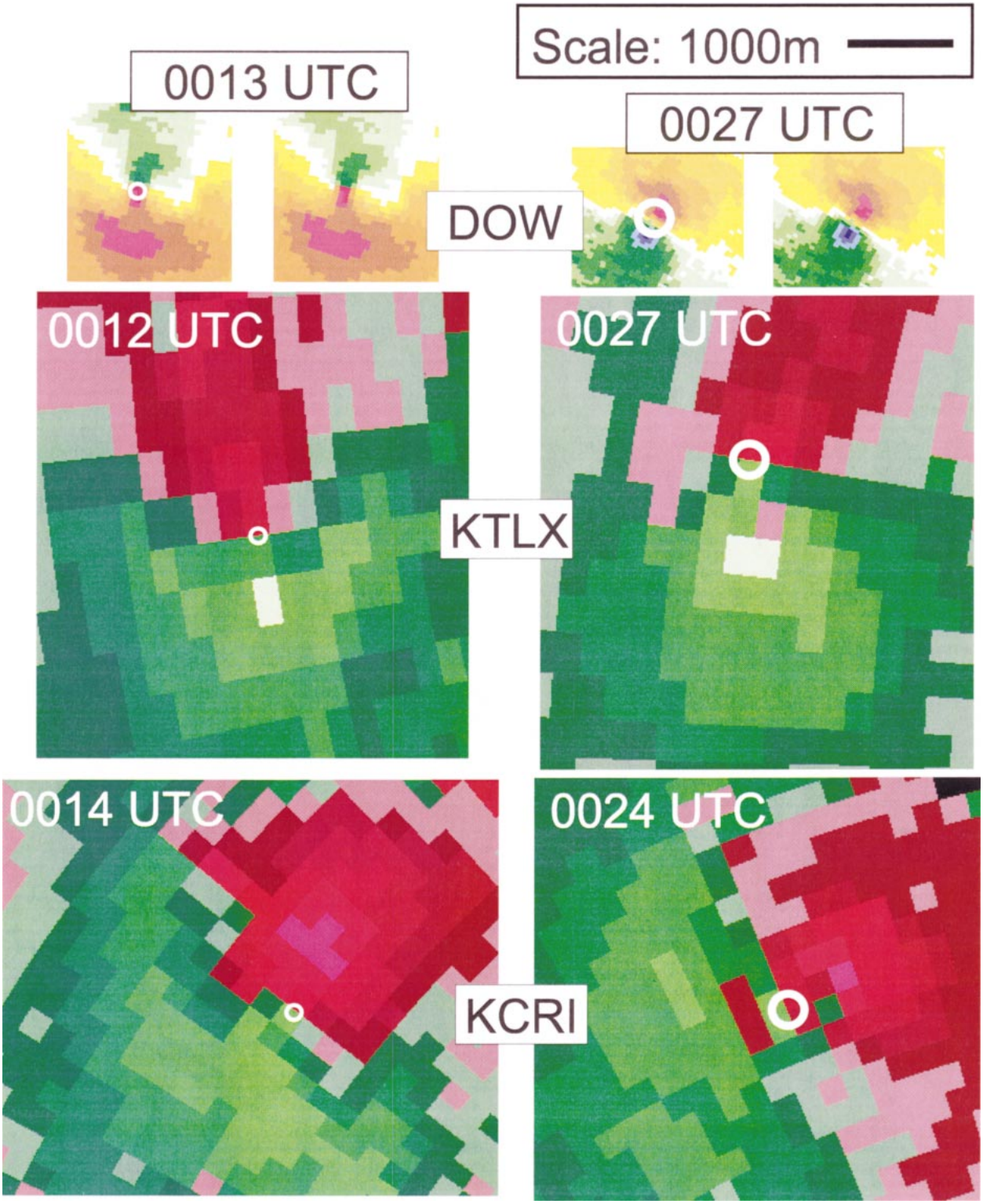

FIG. 14. Comparison of WSR-88D velocity (KTLX and KCRI) and DOW velocity for two different times (0012 and 0024/0027). White circles are estimates of tornado diameter from the DOW. The centers of WSR-88D radar beams are 100–300 m ARL; the centers of DOW radar beams are 50–150 m ARL.

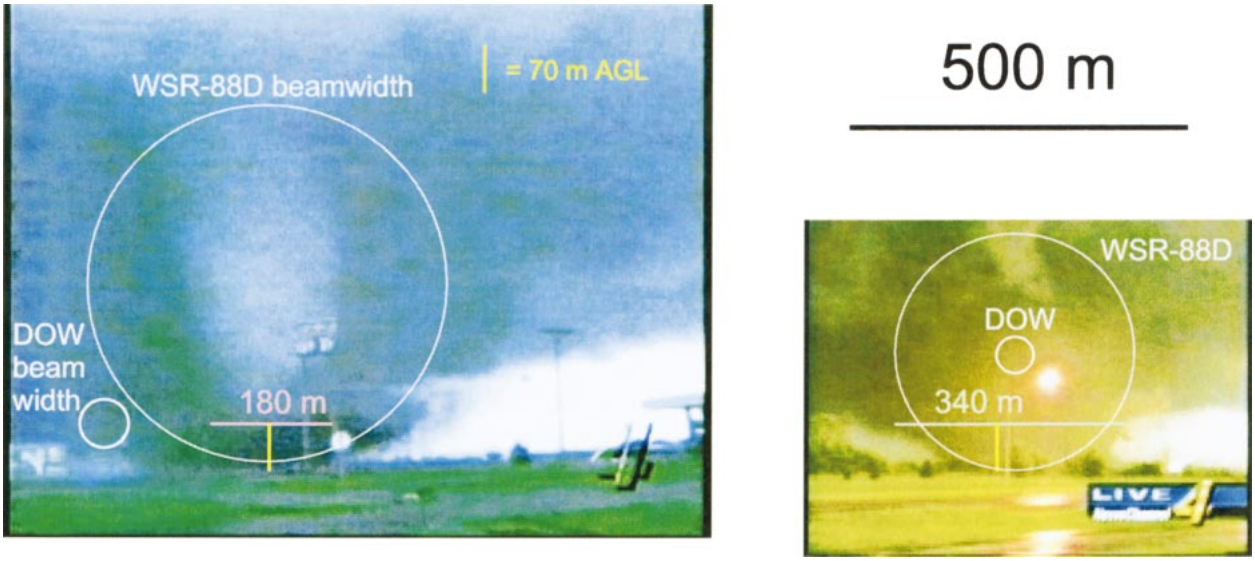

FIG. 15. Tornado images at two times: (left) 0012 and (right) 0028 UTC. Tornado images courtesy of KFOR-TV, Channel 4, Oklahoma City. Images are scaled. Vertical placement of radar beams (assumed to be 1°) is determined by height of lowest elevation angle at correct range to tornado. Horizontal placement of radar beams is arbitrary. At 0012 UTC, DOW (KTLX WSR-988D) range to tornado was 4.1 km (28.0 km). At 0028 UTC, DOW (KTLX WSR-88D) range to tornado was 3.3 km (20.0 km).

nado-like vortices may also give better estimates of peak wind speed.

It has been shown that the WSR-88D has significant problems in sampling a close-range tornado such as the 3 May tornado; even a large tornado at close range is smaller than the size of the radar beam. It was documented that wind speed changes and damage/intensity changes were not resolved well. As a result, it is difficult to suggest that WSR-88D tornado cyclone signatures can be used to infer tornado wind speed and damage/intensity changes. The best use of the WSR-88D, when a TCS or a TVS is present, is to suggest an enhanced probability of a tornado forming or existing. It is unlikely that current sampling limitations will allow absolute confirmation of a tornado or determination of specific tornado intensity or changes in tornado intensity. These conclusions are true for velocity signatures at close range (<60 km) and become even more pronounced as range increases.

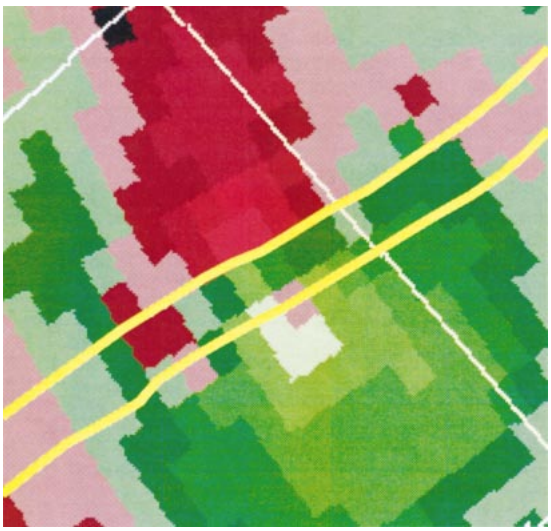

FIG. 16. KTLX WSR-88D velocity signature at 0027 UTC overlain by tornado damage track.

The full understanding of tornado velocity signatures remains elusive. We anticipate that collaboration between University of Oklahoma and NSSL scientists, along with other researchers, will produce additional datasets and provide new understanding of the WSR-88D signatures. As this collaboration occurs, it will lead to enhancement of WSR-88D signature utility in the warning decision-making process.

Acknowledgments. We gratefully acknowledge Greg Stumpf for developing the F-scale contour map and May Yuan for help with preparation of several figures. We thank the many people who aided in radar data collection and processing and participated in the tornado damage survey. We also thank television station KFOR, Channel 4, for use of two of their tornado images. The DOWs are a collaboration between OU and NCAR and are supported by NSF and ONR.

REFERENCES

Agee, E. M., J. T. Snow, and P. R. Clare, 1976: Multiple vortex features in the tornado cyclone and the occurrence of tornado families. *Mon. Wea. Rev.*, **104,** 552–563.

Bluestein, H. B., and A. L. Pazmany, 2000: Observations of tornadoes and other convective phenomena with a mobile 3-mm wavelength, Doppler radar: The spring 1999 field experiment. *Bull. Amer. Meteor. Soc.*, **81,** 2939–2951.

——, W. P. Unruh, J. G. LaDue, H. Stein, and D. Speheger, 1993: Doppler radar wind spectra of supercell tornadoes. *Mon. Wea. Rev.*, **121,** 2200–2221.

——, A. L. Pazmany, J. C. Galloway, and R. E. McIntosh, 1995: Studies of the substructure of severe convective storms using a mobile 3-mm wavelength Doppler radar. *Bull. Amer. Meteor. Soc.*, **76,** 2155–2169.

Brown, R. A., and V. T. Wood, 2000: Enhanced detection of tornadoes on 3 May 1999 using prototype fine-resolution WSR-88D measurements. Preprints, *20th Conf. on Severe Local Storms*, Orlando, FL, Amer. Meteor. Soc., 40–43.

——, L. R. Lemon, and D. W. Burgess, 1978: Tornado detection by pulsed Doppler radar. *Mon. Wea. Rev.*, **106,** 29–38.

Burgess, D. W., R. J. Donaldson Jr., and P. R. Desrochers, 1993: Tornado detection and warning by radar. *The Tornado: Its Structure, Dynamics, Prediction, and Hazards*, *Geophys. Monogr.*, No. 79, Amer. Geophys. Union, 203–221.

Crum, T. D., and R. L. Alberty, 1993: The WSR-88D and the WSR-88D Operational Support Facility. *Bull. Amer. Meteor. Soc.*, **74,** 1669–1687.

Donaldson, R. J., Jr., 1990: Foundations of severe storm detection by radar. *Radar in Meteorology*, D. Atlas, Ed., Amer. Meteor. Soc., 115–121.

Dowell, D. C., J. Wurman, and L. J. Wicker, 2001: Centrifuging of scatterers in tornadoes. Preprints, *30th Conf. on Radar Meteorology*, Munich, Germany, Amer. Meteor. Soc., 307–309.

Fujita, T. T., 1971: Proposed characterization of tornadoes and hurricanes by area and intensity. SMRP Research Paper 91, University of Chicago, Chicago, IL, 42 pp. [Available from Wind Engineering Research Center, Box 41023, Lubbock, TX 79409.]

Gardner, A., K. C. Mehta, L. J. Tanner, Z. Zhou, M. Conder, R. Howard, M. S. Martinez, and S. Weinbeck, 2000: The tornadoes of Oklahoma City of May 3, 1999. Wind Science and Engineering Research Center Rep., Texas Tech University, Lubbock, TX, 38 pp. [Available from Wind Engineering Research Center, Box 41023, Lubbock, TX 79409.]

Garrett, R. A., and V. D. Rockney, 1962: Tornadoes in northeastern Kansas, May 19, 1960. *Mon. Wea. Rev.*, **90,** 231–240.

Golden, J. H., and D. Purcell, 1977: Photogrammetric velocities of the Great Bend, Kansas tornado of 30 August 1974: Accelerations and asymmetries. *Mon. Wea. Rev.*, **105,** 485–492.

Hoecker, W. H., Jr., 1960: Wind speed and air flow pattern in the Dallas tornado of April 2, 1957. *Mon. Wea. Rev.*, **88,** 167–180.

Lemon, L. R., D. W. Burgess, and L. D. Hennington, 1982: A tornado extending to great heights as revealed by Doppler radar. Preprints, *12th Conf. on Severe Local Storms*, San Antonio, TX, Amer. Meteor. Soc., 430–432.

Lewellen, W. S., 1993: Tornado vortex theory. *The Tornado: Its Structure, Dynamics, Prediction, and Hazards*, *Geophys. Monogr.*, No. 79, Amer. Geophys. Union, 19–39.

Magsig, M. A., and J. T. Snow, 1998: Long-distance debris transport by tornadic thunderstorms. Part I: The 7 May 1995 supercell thunderstorm. *Mon. Wea. Rev.*, **126,** 1430–1449.

Marshall, T. P., 2002: Tornado damage survey at Moore, Oklahoma. *Wea. Forecasting*, **17,** 582–598.

McDonald, J. R., 2001: Theodore Fujita: His contribution to tornado knowledge through damage documentation and the Fujita scale. *Bull. Amer. Meteor. Soc.*, **82,** 63–72.

NSSL, 2000: WATADS (WSR-88D Algorithm Testing and Display System) reference guide for version 10.2. 200 pp. [Available from National Severe Storms Laboratory, 1313 Halley Circle, Norman, OK 73069.]

Oye, R., C. Mueller, and S. Smith, 1995: Software for radar translation, visualization, editing, and interpolation. Preprints, *27th Conf. on Radar Meteorology*, Vail, CO, Amer. Meteor. Soc., 359–361.

Speheger, D. A., C. A. Doswell III, and G. J. Stumpf, 2002: The tornadoes of 3 May 1999: Event verification in central Oklahoma and related issues. *Wea. Forecasting*, **17,** 362–381.

Wicker, L. J., and R. B. Wilhelmson, 1993: Numerical simulation of tornadogenesis within a supercell thunderstorm. *The Tornado: Its Structure, Dynamics, Prediction, and Hazards*, *Geophys. Monogr.*, No. 79, Amer. Geophys. Union, 75–88.

Wood, V. T., and R. A. Brown, 1997: Effects of radar sampling on single-Doppler velocity signatures of mesocyclones and tornadoes. *Wea. Forecasting*, **12,** 928–938.

Wurman, J., 2002: The multiple-vortex structure of tornado. *Wea Forecasting*, **17,** 473–505.

——, and S. Gill, 2000: Finescale radar observations of the Dimmit, Texas (2 June 1995), tornado. *Mon. Wea. Rev.*, **128,** 2135–2164.

——, J. M. Straka, and E. N. Rasmussen, 1996: Fine-scale Doppler radar observations of tornadoes. *Science*, **272,** 1774–1777.

——, ——, ——, M. Randall, and A. Zahari, 1997: Design and deployment of a portable, pencil-beam, pulsed, 3-cm Doppler radar. *J. Atmos. Oceanic Technol.*, **14,** 1502–1512.